 AIAA 2013-1799

Initial Investigation of the Benchmark SuperCritical Wing Configuration using Hybrid RANS-LES modeling

Mats Dalenbring[1] and Adam Jirasek[2]
Swedish Defence Research Agency FOI, Stockholm, Sweden, SE-164 90

and
Jennifer Heeg[3] and Pawel Chwalowski[4]
NASA Langley Research Center, Hampton, Virginia, 23665, USA

The Benchmark SuperCritical Wing (BSCW) wind tunnel model served as a semi-blind test case for the 2012 AIAA Aeroelastic Prediction Workshop (AePW). The geometry of the BSCW is simple but the flow field is complex and challenging. The BSCW has moderate separation, buffeting and oscillating shock motion. The result from the first AePW shows that CFD modeling based on RANS is insufficient for accurate physical modeling of this moderately separated flow. This paper presents initial CFD results from using a more suited turbulence resolving hybrid RANS-LES method. The result shows important qualitative improvements with respect to the physical modeling of the flow.

Nomenclature

C_p	=	pressure coefficient
c_{ref}	=	reference chord length (= 16 inches for BSCW)
f	=	frequency, Hz
M	=	Mach number
q	=	dynamic pressure, psf
Re	=	Reynolds number per chord, 1/ft
Re_c	=	Reynolds number based on wing chord
V	=	Freestream velocity
x/c	=	chord location, nondimensionalized by wing chord
y	=	span-wise coordinate
α	=	angle of attack
γ	=	ratio of specific heats (= 1.14 for R-134a, = 1.4 for Air)

Acronyms

AePW	=	Aeroelastic Prediction Workshop
BSCW	=	Benchmark SuperCritical Wing wind tunnel model
CFD	=	Computational Fluid Dynamics
DES	=	Detached Eddy Simulation
FRF	=	Frequency Response Function
HIRENASD	=	High Reynolds Number Aero-Structural Dynamics wind tunnel model
LES	=	Large Eddy Simulation, higher order flow solver
URANS	=	Unsteady Reynolds-Averaged Navier Stokes, most common flow solver

[1] Senior Reseacher, Information- and Aeronautical Systems, Gullfossgatan 6, and AIAA Member.
[2] Senior Reseacher, Information- and Aeronautical Systems, Gullfossgatan 6, and AIAA Member.
[3] Research Engineer, Aeroelastic Branch, Mail Stop 340, AIAA Senior Member.
[4] Research Engineer, Aeroelastic Branch, Mail Stop 340, AIAA Senior Member.

I. Introduction

THE overall motivation for the 2012 Aeroelastic Prediction Workshop (AePW)[1] was to assess the state-of-the-art in aeroelastic modeling capability and the lack of public datasets that can be used for model verification and validation. The AePW is intended as a worldwide forum for joint collaborations in the field of aeroelasticity. The transonic regime was chosen from the start as it is well known that classical aeroelastic tools are lacking predictive capability in this range.

Historically, accurate simulation of high-speed unsteady flow over realistic full-scale geometries has been nearly impossible and aeroelastic considerations are in many cases necessary for success. However, the increasing maturity of computational fluid dynamics (CFD) and the exponential growth of computer power today enable engineers to use more realistic models in their design, development and optimization work. In contrast, aeroelastically scaled wind tunnel model experiments is also not an easy task and, more importantly, expensive flight tests must be kept at a minimum for cost reasons. Provided models with acceptable simulation accuracy, the ultimate question will in the end be the analysis turn around time[2].

As a starting point, basic building blocks for model validation were identified, by the AePW organizing committee, based on existing experimental datasets[3]. The focus in the first workshop was on the unsteady aerodynamics. For this purpose, the AePW workshop selected three supercritical wings: the NASA BSW and BSCW configurations, both experimentally tested in the NASA Transonic Dynamic Tunnel (TDT), and the well known HIRENSASD configuration, tested in the European Transonic Windtunnel (ETW). The HIRENASD and the BSCW have similar and rather simple wing profiles. The HIRENASD wing is statically deformed during wind tunnel test and forced oscillations are applied, corresponding to one of the fundamental wing resonance frequencies. The test conditions used on the HIRENASD wing resulted in a very linear behavior and negligible fluid-structure coupling. The first result from the AePW was presented at the 2013 AIAA Aerospace Science Meeting conference[4,5,6,7].

The Benchmark SuperCritical Wing (BSCW) on the other hand, was chosen as a more challenging semi-blind test case for the AePW. The NASA BSCW is not as extensively published as the HIRENASD dataset, but was released to the public in connection to the workshop. The BSCW has separation and also an oscillating shock but the detailed knowledge about the flow is relatively unknown. Both unforced and forced measurements data sets on the BSCW configuration were released to the AePW. A first set of results were generated by different partners and analyzed at the first 2012 AIAA AePW.

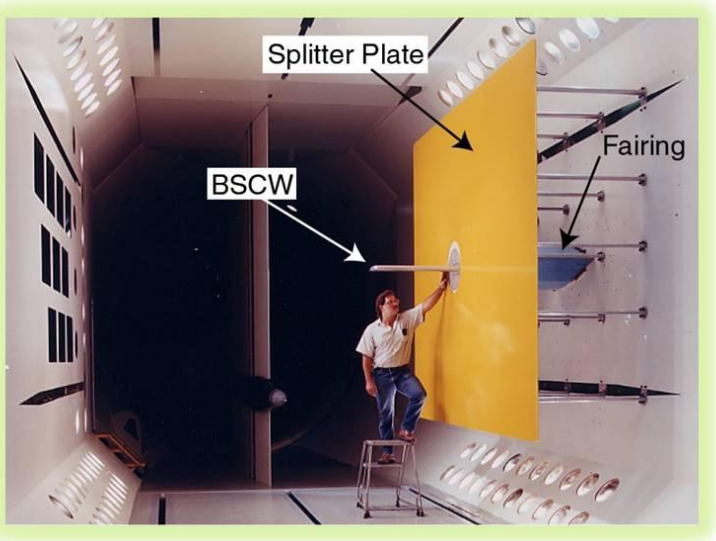

Figure 1. The BSCW mounted in the TDT.

One of the major conclusions pointed out at the first AePW was that there is a systematic error both on the upper part and the lower aft part of the wing, where there is separated flow. Due to the semi-blind character, many analysts chose to use their RANS solver also for analysis of the BSCW test case. A majority of the analyst chose the RANS solver also for this case. It turned out that the BSCW revealed the known fact that RANS methods lose accuracy in cases of separated flow. It was surprising, however, that the effects of the moderate separation for this case caused such significant changes in the model behavior and such significant mismatches between the experimental data and the RANS computations.

As a result of this, a number of analysts pursued a second lap of analysis using RANS-LES hybrid modeling techniques, which is more suited for this type of flow. It is also clear from the AePW that it is necessary to go back and explore the basic assumptions of the unsteady aerodynamic modeling before progressing to coupled aeroelastic system simulations. This paper presents some preliminary results from RANS-LES modeling of the BSCW and comparison with URANS results. Time-accurate URANS solutions were run by analysis teams at FOI and NASA

following the workshop. These new simulation results on the unforced system are compared with experimental data, previously submitted simulation results for the AePW and additional URANS results that are made available.

II. The BSCW case

The experimental data from the BSCW wind tunnel test was released to the AePW analysts following the workshop. For a more detailed description the reader may visit the BSCW experimental data report by Heeg and Piatak[8]. Additional information may also be found in the original NASA reports. The BSCW is a rectangular wing having a 16 inch reference chord length (c_{ref}) and a 32 inch model span, resulting in a total wing area of 512 in^2.

The BSCW was mounted on a large splitter plate, shown in figure 1, located at a distance sufficiently far away from the wind tunnel wall boundary layer, and tested at Mach 0.85. The test medium used in the TDT was R-134a gas and the dynamic pressure was 200 psf, setting the Reynolds number at 4.49 million based on the wing chord. The model pressure instrumentation was limited to one row of pressure transducers, located at the 60% span station. Forced dynamic pressure data were obtained from pitch oscillation motion excitation using an oscillating turntable[9]. Both the 1 and 10 Hz pitch motion excitation case were released to the AePW. An oscillating turn table was used with an angle amplitude of 1° at 5° mean angle of attack. In this paper, only the unforced steady case is investigated.

The results from the AePW for the unforced system case are shown in Figure 2, with the upper and lower surface results plotted separately for clarity. For the AePW, the primary comparison quantity for the unforced system data was the mean value of the pressure coefficient at each of the chord locations where a pressure transducer was located in the experiment. On the plots, each color represents the submitted results from a different analysis team, including grid and time step refinements. The black symbols show the experimental values, with the circles indicating the mode rather than the mean, and the triangles indicating the maximum and minimum values. It is important to note that there is a large range of upper surface shock location predicted by the RANS solutions, with almost all of the predictions indicating a shock position further aft than observed in the experimental data. The pressure distribution over the aft portion of the airfoil is not well-predicted by these computations. This is a region of separated flow, likely extending from the shock to the trailing edge. On the lower surface, the aft load distribution was not well-predicted by the RANS solutions. The BSCW at this condition exhibits a lower surface shock near the 60% chord that is captured by the RANS solutions shown. Aft of the shock, in the region of the supercritical airfoil cusp, the flow is likely separated as indicated by the shape of the pressure distribution for the experimental data. The shape of the mode distribution in this region is not well-captured by the RANS solutions. It is in these areas of separated flow that an improved solution is sought. It should also be mentioned that the RANS solutions, performed for the AePW, were not time-accurate solutions.

Examining the frequency content of the experimental data sets, the blade passage frequency at this condition is 179 Hz. Fundamental structural dynamic frequencies are the: splitter plate vertical mode at 15 Hz, 1st wing bending mode at 21 Hz, 2nd bending mode at 27 Hz and 1st wing torsion mode 80 Hz. In the present CFD analysis the wing is modeled as rigid, excluding any influence of BSCW structural and suspension dynamics. One of the important unsteady flow features that we are trying to define is the frequency content- identified by Strouhal number- associated with shear layer instabilities and vortex shedding, which do couple to structural dynamic motion.

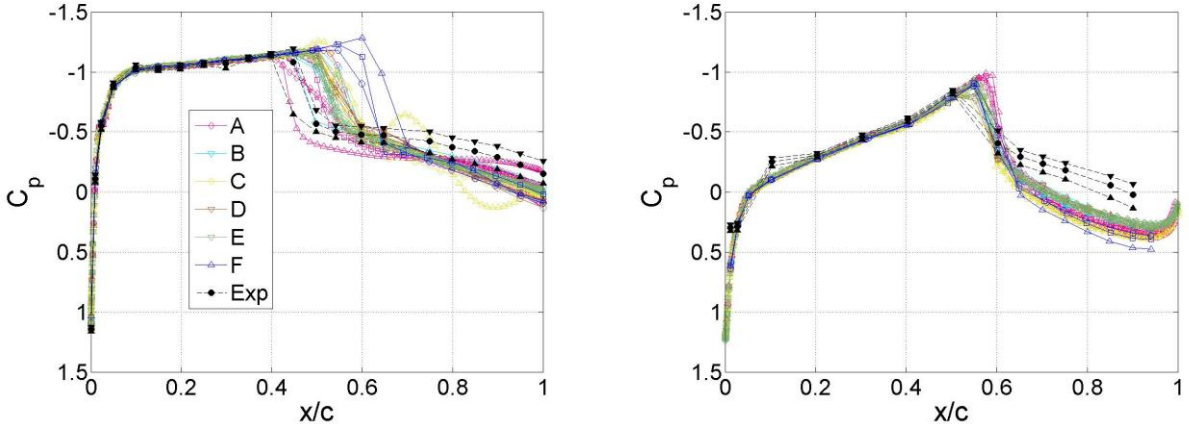

Figure 2. AePW submitted BSCW data-sets for upper surface (left graph) and lower surface (right graph).

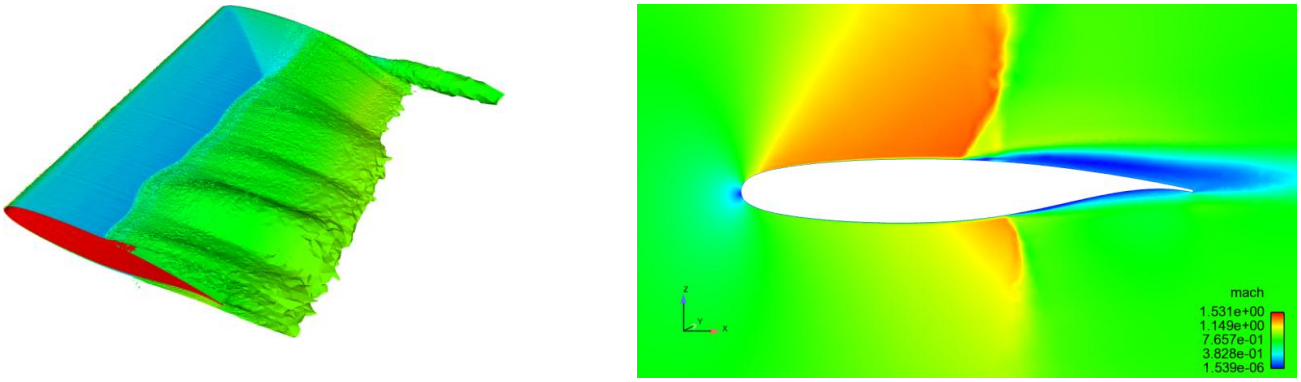

Figure 3. URANS averaged solution iso-surface of vorticity magnitude colored by C_p (left picture).

III. CFD modeling in Edge

The Edge code solves the three-dimensional compressible flow equations on general unstructured grids using an edge-based data structure and node-centered finite volume technique. The edge-based formulation makes it easy to compute any type of element, structured or unstructured. The control volumes are non-overlapping and are formed by a dual grid, which is computed from the control surfaces for each edge of the primary input mesh.

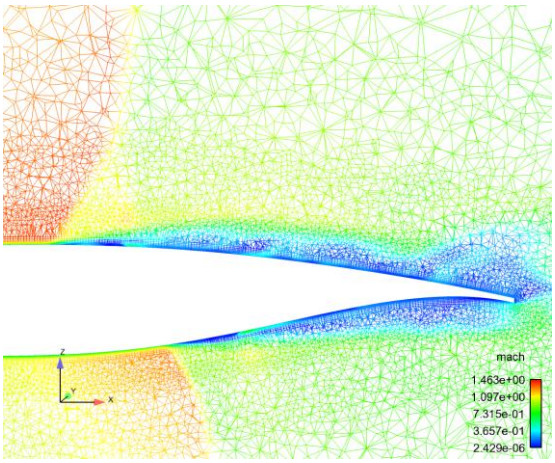

Figure 4. CFD mesh.

In the flow solver, the governing equations are integrated explicitly towards steady state with Runge-Kutta (RK) time integration. Convergence is accelerated using agglomeration multigrid, implicit residual smoothing and line-implicit scheme. Time accurate computations can be performed using dual time stepping scheme that exploits convergence acceleration technique via a steady state inner RK iteration procedure. A variety of turbulence models are available, which are categorized into three different groups, RANS, DES and Large Eddy Simulation (LES) models. The RANS model includes the original one-equation model by Spalart-Allmaras (SAO), and several two-equation models: the Menter SST and Baseline (BSL) models, the Wilcox 1988 k-ω model, the Wallin and Johansson Explicit Algebraic Reynolds-Stress Model (EARSM) implemented within the Hellsten k-ω model, and a Differential Reynolds Stress Model (DRSM).

The DES extension is implemented with the SA model (DES-SA), the HYB0 RANS-LES model[11], and the LES models of Yoshizawa and Smagorinsky [10,11]. The hybrid modeling abandons a full LES resolution of near-wall turbulent flow structures. These regions are instead modeled by RANS model. Away from the wall where massive separation occurs LES is adopted. The HYB0 zero-equation model, adopted throughout in this work, uses a near-wall mixing-length RANS coupled with the Smagorinsky SGS model, where the SGS model coefficients have been calibrated using fully-resolved LES data. The flow solver Edge is primarily developed and maintained by FOI. Since the start of the Edge project in 1997, several academic and research institutes have joined the Edge community as users and developers. Edge is available as a complete source package, subject to the FOI license agreement[12].

IV. Assessment of grid and time step requirements

The information in the literature on establishing appropriate time-step limits for unsteady calculations is relatively sparse, as is the guidance for spatial gridding requirements when applying this aerodynamic modeling. The space-time error balancing often relies on some rule-of-thumb developed into a best-practice. The recent paper by Cummings et al.[12] provides useful insight on this subject. Generally, one would need to understand the flow physics and the time-scales for each specific case. The different scales in the flow are generally interrelated and in order to predict vortex shedding one needs to model also the shear layer instabilities accurately.

Convergence is generally not granted when solving the non-linear Navier Stokes equations, as multiple solution curves exist depending on the flow conditions. Also, the turbulent flow at a given position can not be determined locally as it depends on up-stream flow time history. This is particularly true in the case of massively separated flow.

In this case one can rely only on statistics and sensitivity/stability analysis, based on different grids, time-steps, number of sub-iterations within one time-step and numerical damping values. In resolved LES, Spalart[15] showed that at least five spacial grid points are needed at the smallest flow structures. Given this, there is of course potential for grid adaption and construction of computationally effective grids. The grid used throughout this study is however graded more or less uniformly, according to Figure 4.

The mesh was created using a two-step approach. In the initial step, the ANSYS® ICEM CFD™ was used to generate a surface mesh and an initial volume mesh. In the second step, the initial ICEM mesh was transferred into the in-house mesh generator TRITET to grow the viscous boundary layers. The final inner RANS region is created in TRITET with the advancing front technique. A systematic grid time-step study is of course recommended but was not performed as a part of this study. Mesh size and typical values of the boundary prismatic layers are determined based on pervious in-house RANS-LES experience and best-practice and some gridding guide lines provided by the AePW. The final mesh used in the simulations has a size of about 13 million points, about 900 000 triangles on the wing surface and about 6 cells across the trailing edge. The cell count is: 10 833 047 tetra elements, 21 810 638 prism and 64 012 pyramid elements.

As a rule-of-thumb a time-step $\Delta t^* \leq 0.025$ is recommended as an initial starting point, depending on the flow features at interest. In the present simulations, this corresponds to a non-dimensional time-step Δt^* ($\Delta t^* = \Delta tV/c$) equal to 0.0175 for the unforced system CFD simulations and 0.035 in the 10 Hz forced oscillation case. Provided, the sampling rate is twice the frequency of interest this corresponds to a Stouhal number of 29 and 14 respectively. These frequency values match shear layer instabilities that will trigger large scale flow features as for example vortex shedding. In the simulation dual time stepping is used with 50 sub-iterations for the unforced case and 60 sub-iterations when proceeding to the analysis of the 10 Hz forced BSCW case.

V. Unforced system results

In the CFD simulation of the unforced BSCW the sample rate was set to 20 000 samples/second (Δt = 5e-5 seconds) in Edge, with a length that is currently 6760 time points which corresponds to a 0.338 second long time record. The CFD grid points are divided into upper and lower surface points, putting 686 on the upper and 687 on the lower. The experimental data for the unforced system has 5000 samples, sampled at 1000 samples/sec producing time record length of 5 seconds. On the upper surface, the CFD pressure coefficients are grouped into 4 regions:

1. Leading edge, ahead of the shock, x/c < 0.1;
2. Ahead of the shock, x/c = [0.1 to the shock leading edge position at approximately 0.3736];
3. Shock region, x/c = [0.3736 - 0.475]. The point numbers associated with the shock are #264 - 325;
4. And aft of the shock region, x/c = [0.475, 1]

Example time histories for regions 2, 3 and 4, on the upper surface, are shown in the plots in Figure 5 for the experimental data (subplot a), the Hybrid LES computations (subplot b) and a comparison time-accurate URANS solution provided by NASA using FUN3D[13] (subplot c). It should be noted that the time scale for the URANS solution is 1/10 of the other time scales. At the time of publication, only a very short time record of data had been generated. From these plots, it is seen that the dynamics ahead of the shock (red lines) have substantially lower energy that either of the other locations represented. Both the hybrid LES and the URANS predict the average value well.

The shock oscillations are shown in each plot by the highly non-linear blue traces. The lower negative values of the pressure coefficients form floors in each plot, which show when the sensor of gridpoint is ahead of the shock, on the supersonic plateau. The upward spikes shown for the experimental data and the hybrid LES results indicate the sudden forward movement of the shock as a function of time. The URANS solution has not been run yet for a long enough time to make a similar assessment. In comparison with the experiment, the hybrid LES solution appears to have a higher frequency associated with the oscillatory shock and appears to have lower damping, indicated by the shaper peaks. The frequency content of the hybrid LES and experiment will be examined in detail later in this paper using Fourier analysis. Both simulations appear to predict approximately the same pressure change across the shock, reflected by the difference between the maximum and minimum values of the blue traces.

Aft of the upper surface shock, in the separated flow region, the differences in frequency content are also evident. The URANS solution shows almost no dynamic content, as the yellow line is nearly constant.

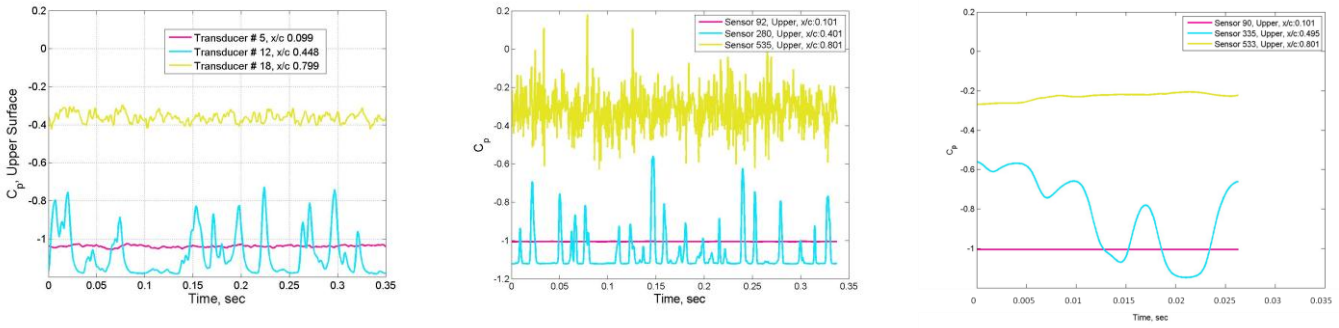

a) Experimental data b) Hybrid LES computations c) URANS computations

Figure 5. C_p vs. time in region 2(red), 3 (blue) and 4 (yellow).

The hybrid LES contains dynamic energy at this location, in excess of the experiment, indicated by the larger magnitude and higher frequency fluctuations. The shock region is plotted in more detail below in Figure 6 for the hybrid LES solution. The detailed plot of the shock oscillations emphasizes the floor behavior described above corresponding to the supersonic plateau. It also shows a pressure ceiling aft of the shock. This ceiling is less constant than the floor due to the separated flow in the aft-of-shock region. The time scale has been zoomed and several sensors (elements) within the region where the shock is active are shown. Sensor 264 is at the forward edge of the shock motion and rarely exhibits any sign of the shock motion. Sensor 334 is aft of the region qualitatively assessed to have shock motion. The mean values are shown in the left graph in Figure 7 below.

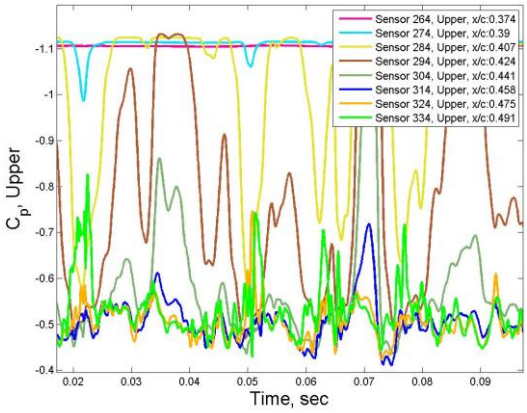

Figure 6. Upper surface pressure coefficient time histories, shock region.

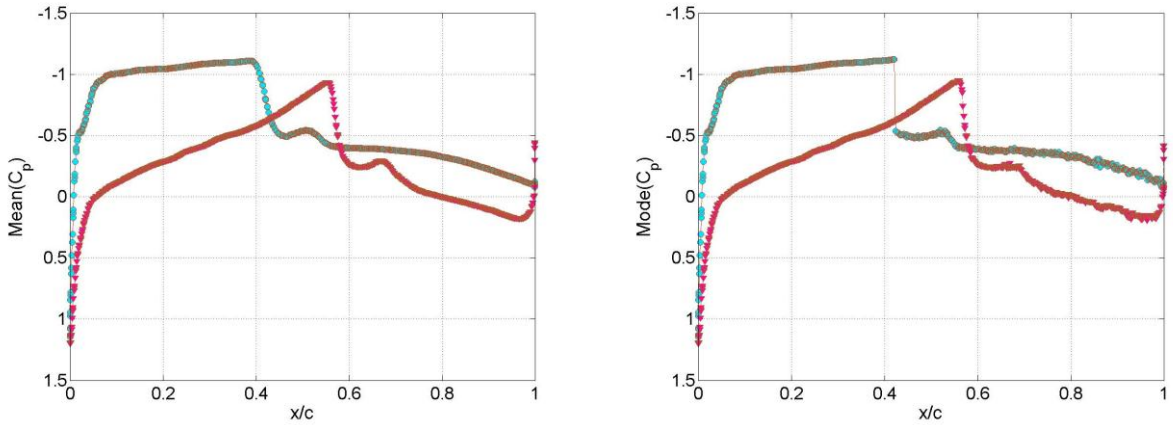

Figure 7. Mean C_p (left graph) and Mode C_p (right graph).

In the right graph of Figure 7, the central (mode) values are shown. The mode was computed at each grid point by generating a histogram, where the number of bins is chosen based on Scott's rule[16]. The mode is reported as the central value of the most popular bin. With this number of time points, 6760, the number of bins used is 51. Note that the shock sharpens when the mode is considered, rather than the mean.

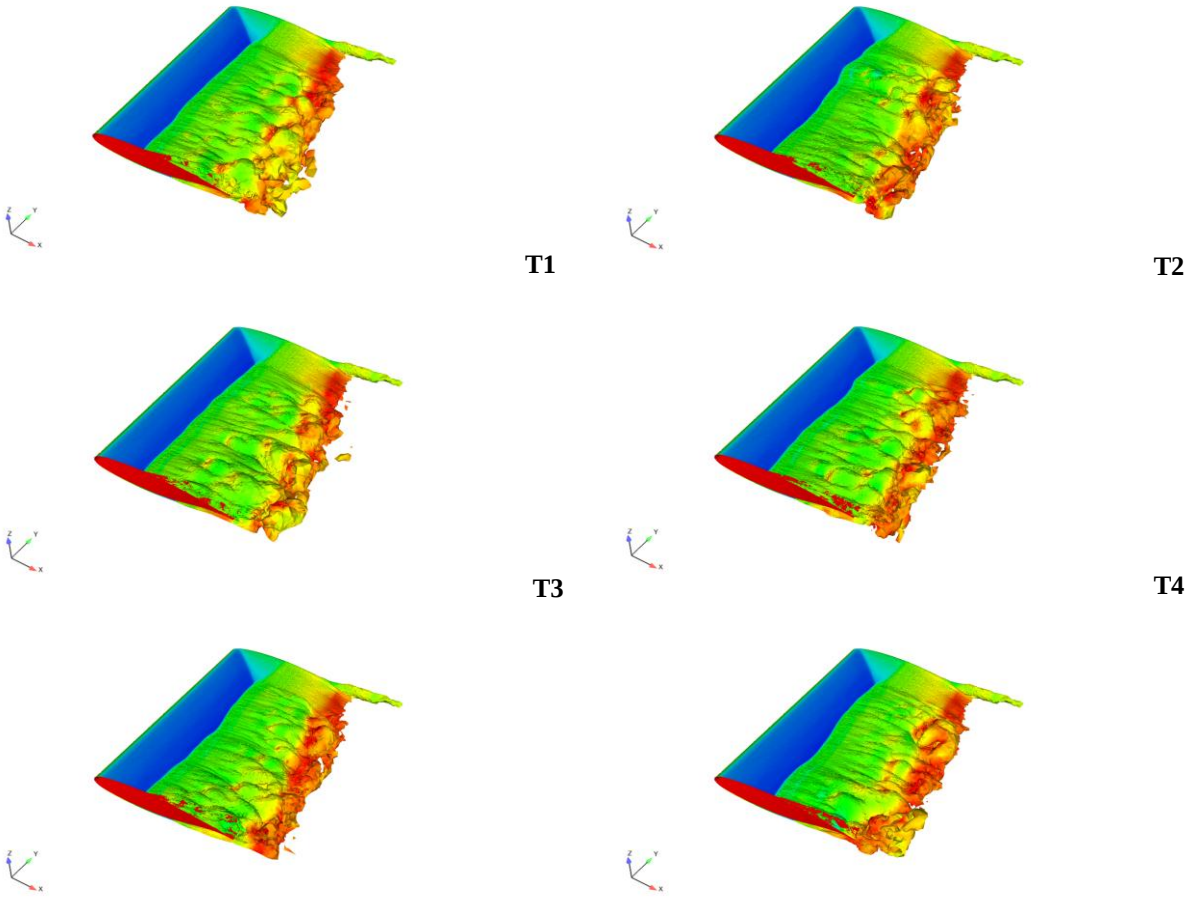

Figure 8. Snapshots of flow field vorticity colored by C_p, at time T1 - T6 marked by red dots in Figure7.

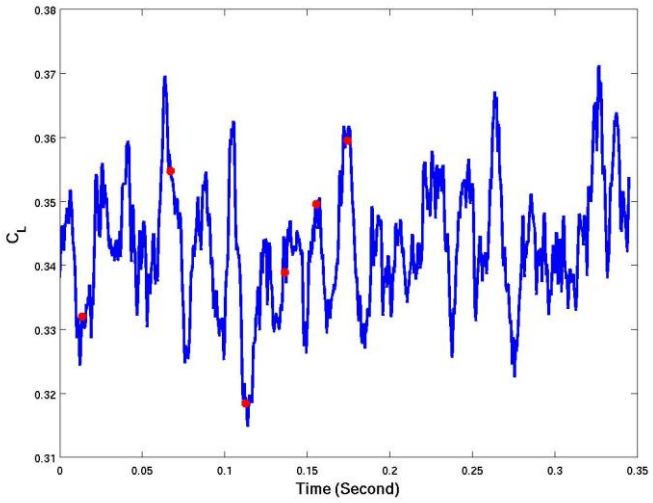

Figure 9. Time history of the integrated lift coefficient C_L.

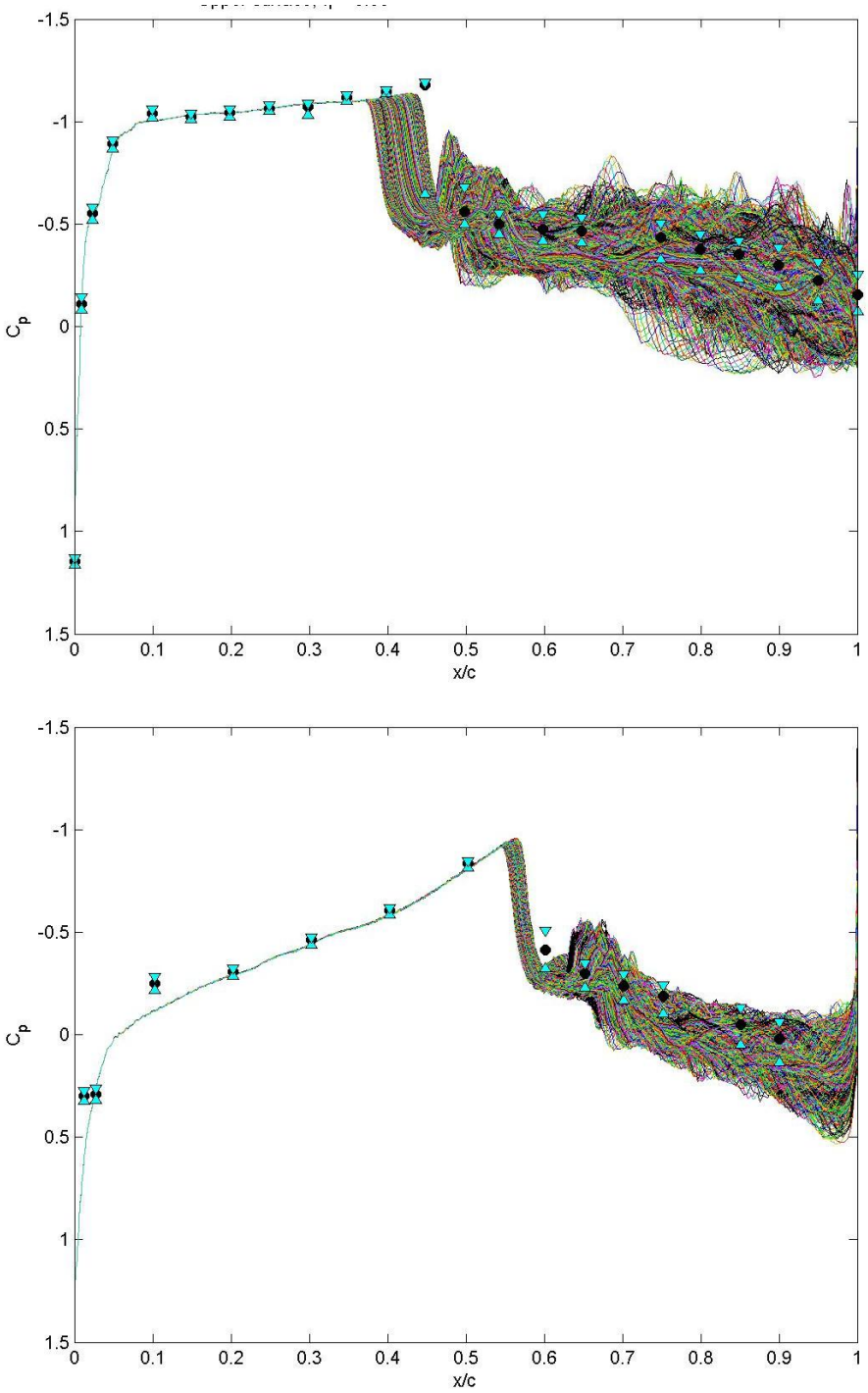

Figure 10. Measured upper surface C_p with max-min bounds and all CFD data point (upper graph) and corresponding data for the lower surface (plotted in the lower graph).

In Figure 8, the instantaneous flow field is visualized, with corresponding time marked by red dots in Figure 9. Note here the span wise shock position, oscillating shock motion and the flow features of the separated area behind the shock. For comparison, URANS simulation results using Edge is also shown in Figure 3.The upper graph in Figure 10, shows all CFD point time histories and corresponding 22 wind tunnel measurements points; with mean value and max-min bounds plotted, for the upper surface. The lower graph in Figure 9 shows the corresponding lower surface.

These plots emphasize the increased dynamics calculated in the separated flow regions as well as the difference in the chord-wise location of the shock oscillation region. The upper surface shock is shown to oscillate forward of the experimental configuration's shock oscillation region. On the lower surface, this is more difficult to assess due to the distance between pressure transducers in the vicinity of the shock.

The URANS solutions for the unforced BSCW configuration were not performed in a time-accurate manner for the AePW as discussed previously. However, several analysis teams opted to perform time-accurate simulations using URANS following the workshop. One of those solutions is used here as a benchmark to illustrate the differences between the URANS solutions and the hybrid LES results. These comparisons are presented in Figure 11, along with experimental data. In this figure, the mode of the experimental data is shown by the black line and symbols; the minimum and maximum are shown by the grey lines. The mode of the time-accurate URANS solution is shown by the darker blue line, with the minimum and maximum indicated by the lighter blue lines. The URANS solutions show the upper surface shock location further aft than the experimental data and do not show a great deal of variation on the upper surface, aft of the shock. Variation in this region is an indicator of the dynamic content.

The hybrid LES results are shown by the red line (mode) and pink lines (minimum and maximum). The range of the solution aft of the shock indicates that the dynamics are being overpredicted by the hybrid LES in the separated flow region. Note, however, that the distributions of mode on both the upper and lower surfaces in the separated flow regions agree better with the experimental data than the URANS solutions.

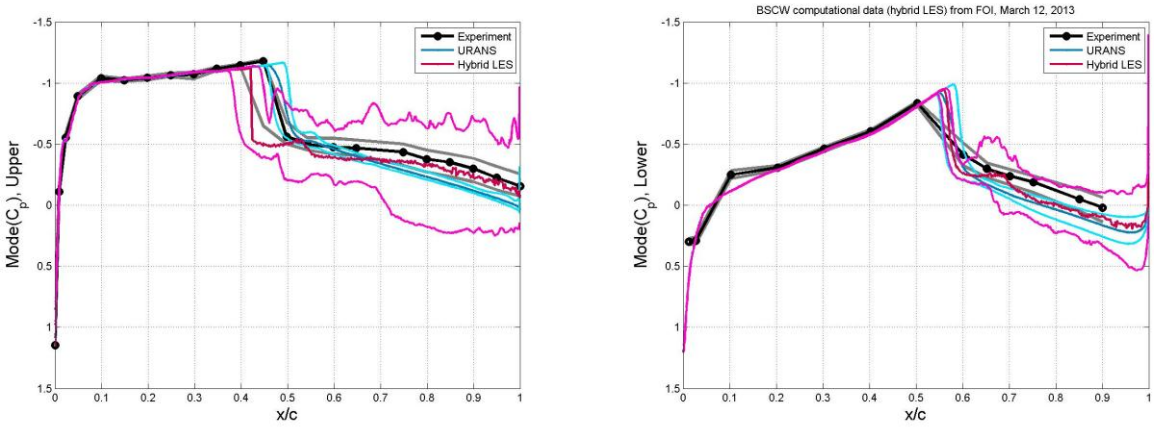

Figure 11 . Comparison of experimental data, URANS and hybrid LES results; mode of C_p.

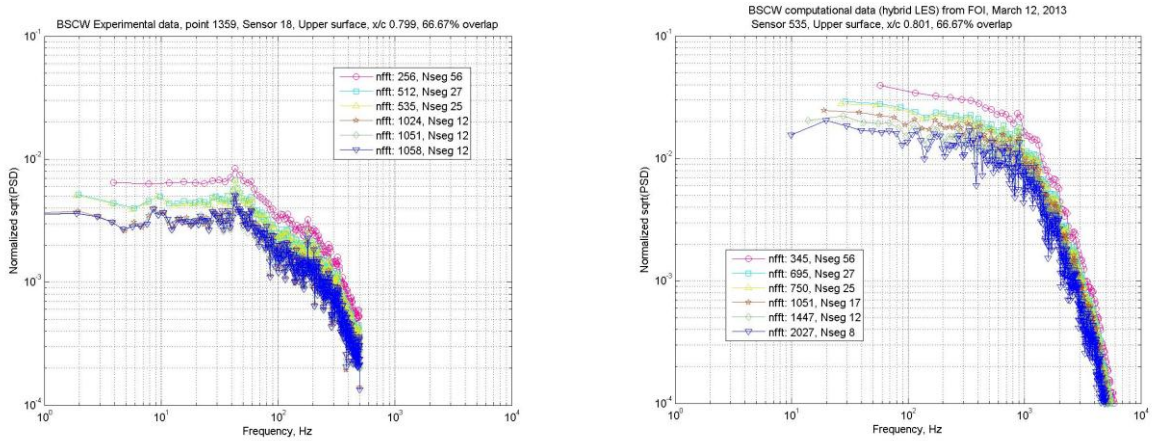

Figure 12. PSD spectrum using different record lengths forward (left graph) and aft shock (right graph).

In order to judge the level of model agreement it is helpful to look also at the frequency content of the signal. The upper surface data of the wing is analyzed first.

We want to compare the computational results with the experimental data. One problem is that we have a very short CFD time record (0.338 seconds), which makes resolving the lower frequencies in the computational data troublesome.

Conversely, the sample rate for the experimental data is much lower (1000 samples/second), so we can not see the higher frequencies in the experimental data. The two plots in Figure 12 show experimental and computational data on identical axes for the x/c = 0.8 location, which is located in the separated flow region.

Experimental data is plotted on the left and CFD result is on the right. The processing parameters are not the same. The processing parameters for the LES data shown: the largest time record possible (6760 points) shown by the ragged blue line, and then with window lengths of in the vicinity of 2048 points shown by the large grouping, and then by 512 and 256 shown by the turquoise (cyan) and raspberry(magenta) lines. The shapes are different and it is intractable to find frequencies in common, possibly due to the time record length and the sample rate mismatches. The CFD results seem to be an order of magnitude higher at the low frequencies. The knee in the FRF appears to be near 40 Hz for the experiment and near 900 Hz for the computational results. There is another knee in the experimental data near 200 Hz.

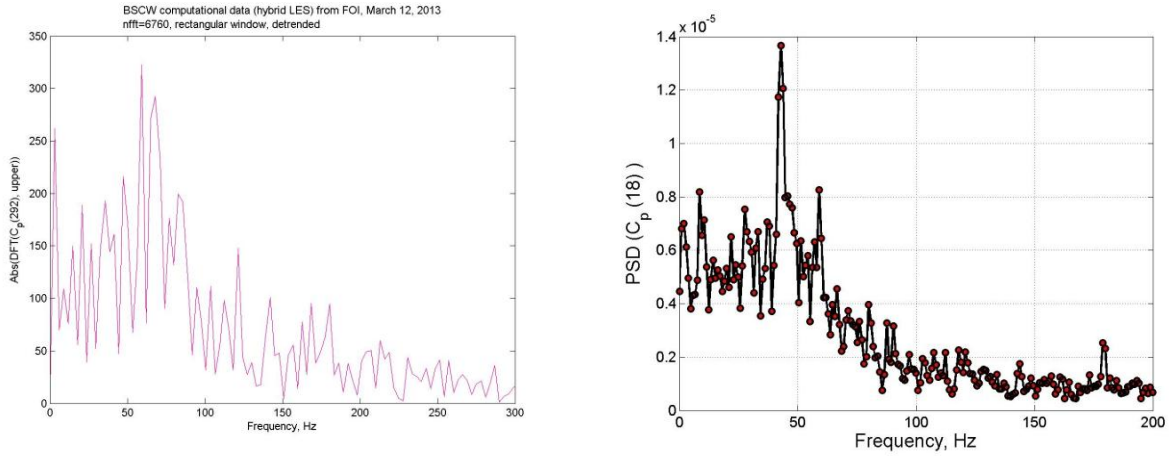

Figure 13. Spectrum C_p aft shock CFD (left graph) and measurements (right graph).

The absolute value of the discrete Fourier transform (DFT) coefficients for element number 292 is plotted in Figure 13 (left graph). Element 292 has the most maximum DFT points out of all sensors, evaluating the maximum over the range from 0 to 300 Hz. Note that element 292 is in the range of the oscillating shock. For comparison the PSD for transducer number 18 from the experimental data is also plotted in Figure 13. Note here the strong peak at around 50 Hz, visible in both experiments and the CFD simulations.

The computational data was further analyzed in the frequency domain, computing PSDs; a subset of the sensors are shown below in Figures 14 (upper surface) and 15 (lower surface). The PSD for each of the experimental data transducers is plotted and the element from the CFD solution that was nearest in terms of x/c. Choosing the experiment-computation correspondence in this way, there is an expected mismatch near the shock, since the shock location is being predicted to be located towards the leading edge, relative to the experimental data. For the results shown, the experimental data was processed using block size 1051 and the CFD data was processed using block size 1447. Hanning windowing was applied to all data blocks, with 67% overlap.

All results in these comparisons, shown below in Figure 14 and 15, are normalized to account for different sample rates and block sizes. All analyses used Hanning windowing. Note here the peak at 179 Hz corresponding to the wind tunnel blade passage frequency.

The PSD results show up in the groupings described at the beginning of the time history discussion. The PSDs of leading edge elements go to the very low values at the high frequencies, the forward elements PSDs still go to a low value plateau, the PSDs of elements in the shock-oscillation region are shown by the transitional looking traces and the aft elements are shown by the traces that drop off at the higher frequencies.

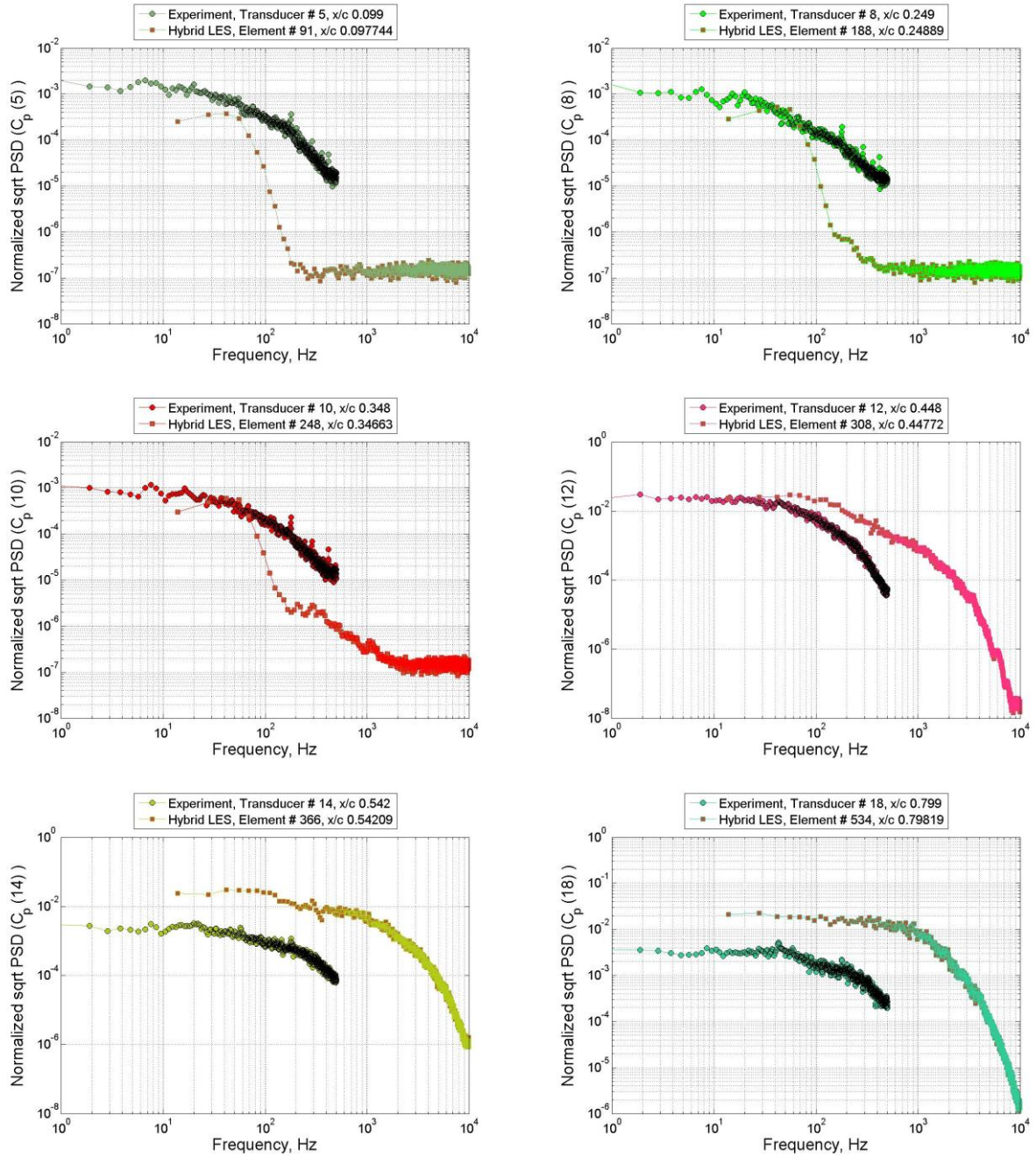

Figure 14. Measured and CFD computed spectrums at different upper surface transducer locations (5, 8, 10, 12, 14 and 18).

For locations ahead of the shock, the PSD of the experimental data is greater than the computational data. For locations at and aft of the shock, the PSD of the experimental data is less than the computational data. The high frequency shapes of the PSD's are similar, but offset, both in magnitude and frequency. These characteristics confirm the earlier comments regarding the dynamic energy content in the different regions of the flow field in the simulation and experiment. The hybrid LES is overpredicting the dynamic content in the oscillating shock regions and the separated flow regions.

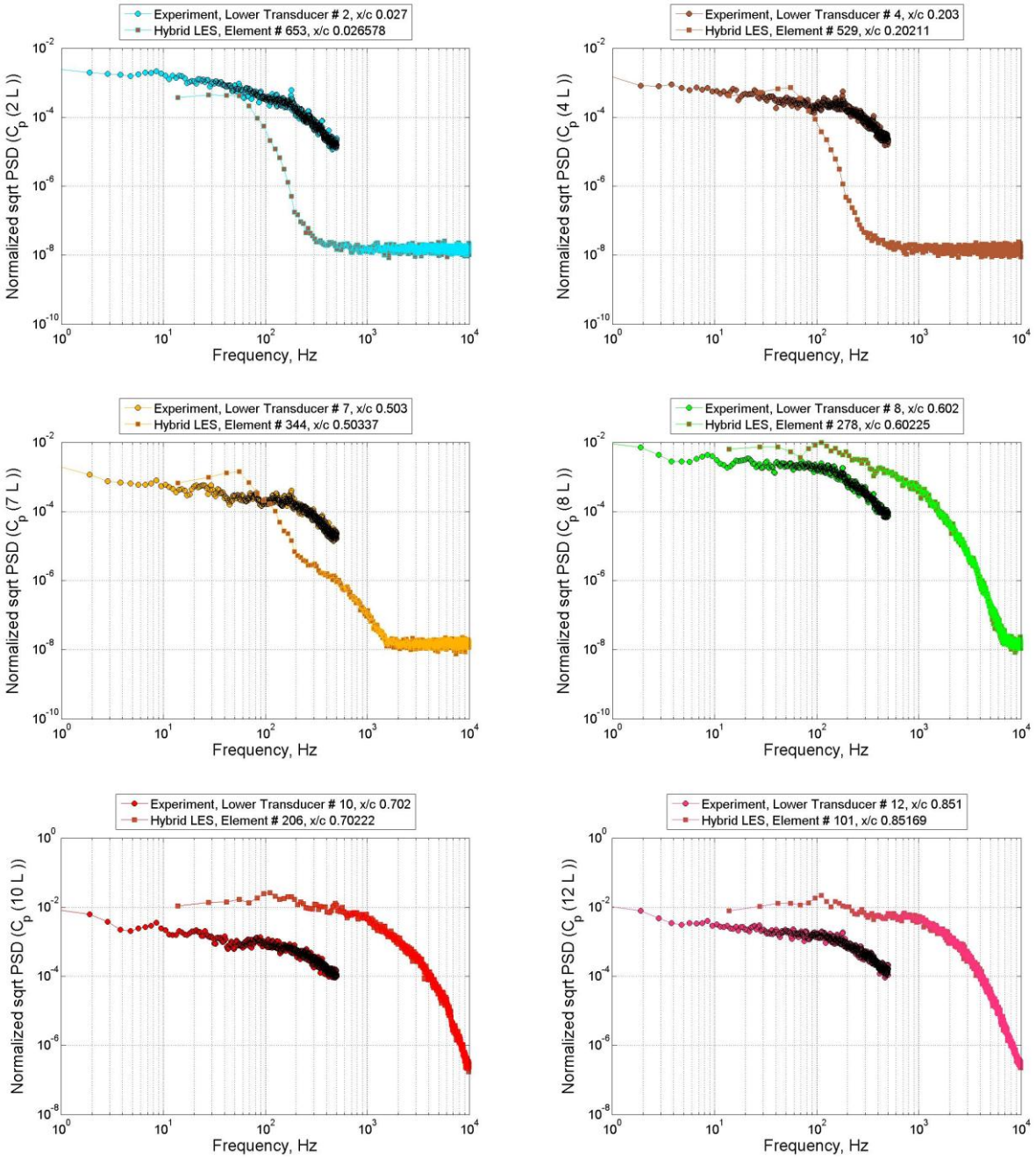

Figure 15. Measured and CFD computed spectrums at different lower surface transducer locations (2,4,7,8,10 and 12).

An essential step in sorting out the dynamic content and the underlying physical sources of modes observed is to examine the wind tunnel turbulence spectrum. In Figure 16 below, an example plot of data obtained in performing wind tunnel turbulence quantification is shown. This data set is detailed in reference 17. For this test, at this condition, the blade passage frequency was near 153 Hz, but the mode is washed out of this data for reasons not investigated or discussed in the reference. The blade passage frequency is different for the empty tunnel turbulence testing principally due to the tunnel blockage that is present in the BSCW test. The turbulence data also shows a prominent mode near 55 Hz and prominent knees in the data near 600 and 2500 Hz.

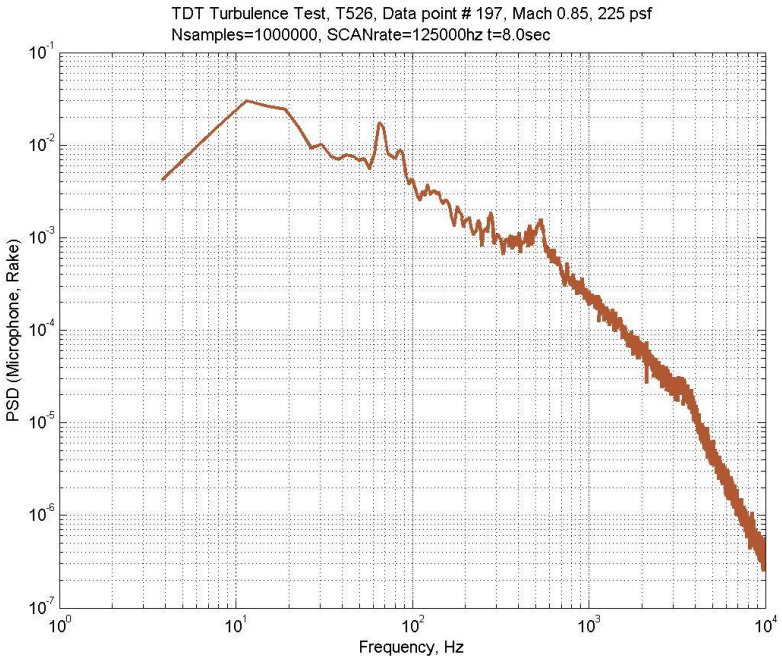

Figure 16. TDT wind tunnel turbulence PDS, microphone at rake position.

To date, we have not established causal relationships between the wind tunnel turbulence spectrum and peaks observed in BSCW PSDs.

VI. Discussion

The results presented in this paper are initial results from using a more turbulence-resolving CFD method to capture the flow physics of the BSCW. The result presented here shows significant improvement compared to URANS. The previous solutions of the BSCW, generated with URANS solvers, lacked the dynamic energy in the separated flow regions that was observed in the experimental data. URANS solutions predicted the upper surface shock location too far aft and the lower surface aft pressure distribution too convex. The present hybrid LES analysis has demonstrated improvements in each of these areas. The current simulation, however, appear to overpredict the magnitude and frequency of the dynamic content, and the shock has moved further towards the airfoil leading edge than the experimental data.

Another difference between measured and simulated PSD spectra exists with regard to the information ahead of the shock. While the dynamic content ahead of the shock is small relative to the magnitude aft of the shock, substantial discrepancies in frequency content exist in this region when comparing the hybrid LES compuations and experiment. The PSDs seems to not capture very well the high frequencies in the thin boundary layer. We suspect four underlying reasons for this:

1. The mesh is likely too coarse for aeroacoustic simulation, eliminating the possibility of modeling small eddies
2. The free-stream wind tunnel turbulence is providing an excitation spectrum to the wind tunnel model that is not captured in the simulation
3. Elastic vibrations of the model
4. CFD boundary conditions

We believe that issues numbered 2 and 3 are more important as the leading edge boundary layer is very thin. Moreover, it seems that once we get to separated flow, the shape of the PSD spectra is similar but with an offset. The similarity is because of the flow separation and possibly all small eddies are predicted fairly well which would somehow milden the first statement about a coarse mesh, although we believe the mesh of for aeroacoustics is too coarse.

Regarding the wind tunnel turbulence, there are screens at the forward turning vane locations to smooth the flow. Wind tunnel turbulence data can give some insight into the noise level- more importantly, though, into the frequency range of turbulent content. As we move forward with this investigation, we hope to better understand and utilize the turbulence test results.

When looking at the frequency content of the PSDs associated with the hybrid LES solutions, in the separated flow regions there is a relatively consistent roll off that intiates near 100 Hz. This corresponds to a Strouhal number of 0.28, which is within the range of typical values reported for buffeting of wings in separated flow. The present CFD analysis is done without a structural dynamic model; the wind tunnel model is assumed rigid in all computations to date. This may be one source of the discrepancies observed between computations and experiment. Also, an inviscid boundary condition is used on the splitter plate in the CFD analysis, which has been observed in other configurations to have significant influence on the results.

At last, is there a large cost penalty associated with switching from URANS to the HYB0 model? Provided that we have equal mesh and time-step the cost will in fact be slightly lower due to the use of the zero-equation HYB0 modeling technique. On the other hand, as a sacrifice for improved accuracy compared to URANS, turbulence resolving CFD simulations will generally require very small time-steps. In terms of computational cost, the BSCW CFD simulations need to be performed using massive parallel computing in order to produce acceptable solution times. The total solution time for this particular case was in the order of 3 weeks, when using 128 cores on the computer cluster. Another challenge when performing these kinds of simulations is the visualization of data and enormous amount of data collected. In our case, the total amount data stored is close to 10 Terabytes.

Acknowledgments

The authors gratefully acknowledge the AePW team, particularly the BSCW analysts and the AePW Organizing Committee for their guidance and discussions.

References

[1] Heeg, J.; et al, "Plans for an Aeroelastic Prediction Workshop," IFASD-2011-110, International Forum on Aeroelasticity & Structural Dynamics, June 2011, Paris.

[2] Yurkovich, R., "Status of Unsteady Aerodynamic Prediction for Flutter of High-Performance Aircraft", Journal of Aircraft, Vol. 40, No. 5, September-October 2003.

[3] "https://c3.nasa.gov/dashlink/projects/47/", January 2013.

[4] Heeg, J., Chwalowski, P., Florance, J.P., Wieseman, C.D., Schuster, D.M., and Perry, B. III, "Overview of the Aeroelastic Prediction Workshop," AIAA 2013-0783, 51st AIAA Aerospace Sciences Meeting, January 7-10, 2013, Texas.

[5] Schuster, D.M., Heeg, J., Wieseman, C.D., and Chwalowski, P., "Analysis of test case computations and experiments for the Aeroelastic Prediction Workshop," AIAA-2013-0788.

[6] Heeg, J., Chwalowski, P., Wieseman, C.D., Florance, J.P., and Schuster, D.M., "Lessons learned in the selection and development of test cases for the Aeroelastic Prediction Workshop: Rectangular Supercritical Wing," AIAA-2013-0784, 51st AIAA Aerospace Sciences Meeting, January 7-10, 2013, Grapevine, Texas.

[7] Schuster, D., Chwalowski, P., Heeg, J., and Wieseman, C., "Summary of data and findings from the First Aeroelastic Prediction Workshop," Tech. rep., Hawaii, 2012, 7th International Conference on Computational Fluid Dynamics, ICCFD7-2012.

[8] Heeg, J. and Piatak, D.J., "Experimental data from the Benchmark SuperCritical Wing wind tunnel test on an oscillating turntable," to be presented at the 54th AIAA/ASME/ASCE/AHS/ASC Structures, Structural Dynamics and Materials Conference, April 8-11, 2013, Boston.

[9] Piatak, D.J., and Cleckner, C.S., "Oscillating Turntable for the Measurement of Unsteady Aerodynamic Phenomenon, Journal of Aircraft, Vol 14, No. 1, Jan. –Feb. 2003.

[10] Peng, S-H, "Hybrid RANS-LES Modeling Based on Zero- and One-Equation Models for Turbulent Flow Simulation", Proceedings of 4th International Symposium on Turbulence and Shear Flow Phenomena, Vol. 3, pp 1159-1164, Williamsburg, VA USA, 27-29 June, 2005.

[11] Peng, S-H, "Algebraic Hybrid RANS-LES Modelling Applied to Incompressible and Compressible Turbulent Flows", 36th AIAA Fluid Dynamics Conference and Exhibit, AIAA 2006-3910, 5-8 June, 2006, San Francisco, California.

[12] www.foi.se/edge

[13] http://fun3d.larc.nasa.gov

[14] Cummings, R. M., Morton, S. A., and Mc Daniel, D. R., "Experiences in accurately predicting time-dependent flows", Progress in Aerospace Sciences 44, 241-257, 2008.

[15] Spalart PR. "Young person's guide to detached-eddy simulation grids", NASA C 2001-211032, July, 2001.

[16] Scott, D. W., "On Optimal and Data-Based Histograms,"*Biometrika*, 66, 605-610, Dec. 1979.

[17] Wieseman, C. D. and Sleeper, R. K., "Measurements of Flow Turbulence in the NASA Langley Transonic Dynamics Tunnel", NASA TM 2005-213529, Feb., 2005.